Journal of Sound and Vibration 329 (2010) 247–260

Contents lists available at ScienceDirect

Journal of Sound and Vibration

journal homepage: www.elsevier.com/locate/jsvi

A new type of semi-active hydraulic engine mount using controllable area of inertia track

Thanh Quoc Truong, Kyoung Kwan Ahn *

Graduate School of Mechanical and Automotive Engineering, University of Ulsan, San 29, Muger 2dong, Nam-gu, Ulsan, 680-764, Republic of Korea

ARTICLE INFO

Article history:
Received 3 November 2008
Received in revised form
5 September 2009
Accepted 15 September 2009
Handling Editor: J. Lam
Available online 8 October 2009

ABSTRACT

Automotive engine mounts function to constrain the engine shake motion resulting at low-frequencies, as well as to isolate noises and vibrations generated by the engine with unbalanced disturbances at the high frequencies. The property of the mount depends on vibration amplitude and excitation frequency. It means that the excitation amplitude is large in low excitation frequency range and small in high frequency range. In this paper, a new hydraulic engine mount with a controllable area of inertia track is proposed and investigated. Theoretical works with the mount model to isolate the engine-related vibrations were conducted by an optimal algorithm to control the area of the inertia track under shocks and multi-signal force excitations. This research clearly gives an analysis of the considerable changes in the mount dynamic properties according to the changes in the inertia track area. Consequently, when the inertia track area is tuned, the transmissibility of the mount is effectively reduced.

1. Introduction

Automotive engine mounts are required to constrain engine shaking motions resulting from shock excitations, and also to isolate noises and disturbed vibrations generated by the unbalanced engine. The engine shake vibration frequency is low with a large vibration amplitude, whereas the vibration frequency of the unbalanced engine is high with a small vibration amplitude. High damping and stiffness are needed to reduce the engine shake vibration; however, low damping and stiffness are required to reduce the noises and unbalanced vibrations [1-3]. Damping of using a conventional rubber is not enough to isolate the engine shake. Therefore, hydraulic mounts with inertia tracks have been developed both to increase the damping in the low frequency range and to reduce unbalanced vibrations [4–7]. However, the hydraulic mounts have resonance peaks created by the fluid flow. To reduce these resonance peaks, a decoupler needs to be inserted in the hydraulic mount.

In addition, semi-active and active hydraulic mounts have been developed in order to increase the performance of the passive hydraulic mount [8–16]. A typical example of both the stiffness and damping control system was reported by [11]. In this semi-active hydraulic mount system equipped with an external bleed, the system resonant frequency was controlled by changing the system equivalent spring constant, and the damping is controlled by changing the fluid injection pressure and restricting the orifices. Electro-rheological (ER) fluids have received attention in terms of their use for semi-active control of engine mounts, due to their rapid change in viscosity properties when an electric field is applied. These properties can be easily used to control the system damping. Another type of hydraulic engine mount, which has a varying

* Corresponding author. Tel.: +82 52 259 2282; fax: +82 52 259 1680.
E-mail address: kkahn@ulsan.ac.kr (K.K. Ahn).

0022-460X/$ - see front matter © 2009 Elsevier Ltd. All rights reserved.
doi:10.1016/j.jsv.2009.09.015

Nomenclature

A_p	effective piston area
A_{i0}	average cross-sectional area of the inertia track as in an optimal passive mount
A_i	average cross-sectional area of the inertia track ($=\eta \cdot A_{i0}$)
B_{vt}	volumetric damping in the top chamber (=0)
B_{vb}	volumetric damping in the bottom chamber (=0)
R_r	rubber damping coefficient in the top chamber
R_{i0}	resistance in the inertia track as in an optimal passive mount
R_i	resistance in the inertia track
C_1	compliance in the top chamber ($1/K_{vt}$)
C_2	compliance in the bottom chamber ($1/K_{bt}$)
C_i	viscous damping coefficient in the inertia track ($A_i^2 R_i$)
d_h	hydraulic diameter of the inertia track ($4A_i/P$)
F_{in_O}	input force with the inertia track opened
F_{t_O}	transmitted force with the inertia track opened
F_{in_C}	input force with the inertia track closed
F_{t_C}	transmitted force with the inertia track closed
Ii	inertia of the inertia track ($\rho L_i/A_i$)
K_1	volumetric stiffness in the top chamber (Ap^2/C_1)
K_2,	volumetric stiffness in the bottom chamber (Ap^2/C_2)
K_{bt},	bottom chamber volumetric or bulge stiffness, N/m^5
K_{vt},	top chamber volumetric or bulge stiffness, N/m^5
K_r	rubber stiffness coefficients in the top chamber
K^*	dynamic stiffness
K'	real part of the dynamic stiffness K^*
K''	imaginary part of the dynamic stiffness K^*
L_i	inertia track length
M_e	engine mass
M_i	fluid flow mass in the inertia track ($=Ai^2 Ii$)
P	wetted perimeter of the inertia track
R_{i0}	resistance in the inertia track as in an optimal passive mount
R_i	resistance in the inertia track
s	Laplace operator
T_F	transmissibility
T_{RD}	relative transmissibility
x_e	displacement of engine mass
x_i	displacement of fluid flow mass in the inertia track
η	ratio area of the inertia track
μ	fluid viscosity
ρ	fluid density
ω	vibration frequency

inertia track length and an effective decoupler area is described in [12]. In most cases, damping control is preferred because of its simplicity. Since semi-active mounts have many advantages over active mounts in term of structural simplicity, performance reliability, required power and cost, many researches have focused on developing new mount types working as semi-active mounts. Most control strategies for semi-active vibration isolation systems are developed based on optimal control algorithms. Furthermore, some adaptive control methods can minimize the defined performance index, but may not have the good capability to adapt to significant changes in the excitation signal and system parameters.

Much work has been carried out in the past decade in the field of engine mount isolation and vibration, focusing on the development of engine mount mechanisms and using intelligent control algorithms in order to reduce or cancel the vibration.

In this paper, a new type of hydraulic mount with a controllable area of the inertia track is proposed, and an optimal algorithm to control in the shock excitation and multi-signal excitation is considered. The design parameters of the hydraulic mount's inertia track area represent the performance of the mount with the most sensitivity. When the inertia track area is changed, the dynamic properties of mount are greatly altered. The results obtained from the numerical simulations show that the mount's vibration isolation is greatly affected by tuning the inertia track area.

Hence, a new mechanism model and a mathematic model of a hydraulic engine mount are described in Section 2. The viscosity characteristic of fluid in the inertia tracks and the mount's dynamics response are explained in Section 3. The optimal algorithm control is proposed in Section 4. Section 5 presenting the simulation results for both a single-signal and a multi-signal of the excitation force is considered. Section 6 gives the conclusions of the research and some discussions.

2. Mathematical model of the hydraulic mount with the controllable area of the inertia track

The semi-active hydraulic engine mount is proposed in Fig. 1(a). This mount consists of a rubber structure with two fluid chambers, an upper chamber (main chamber) and a lower chamber (compression chamber), and a controllable inertia track area. The area is controlled by using a linear actuator. The fluid flows from the top chamber to the bottom chamber through the inertia track as shown in Fig. 1(b). The area changes through the displacement of a moving disk. According to the position of the moving disk, the area value is computed by a linear relationship. There are two limit sensors used to set the limited positions of the moving disk. The upper-limit position and the under-limit position of the moving disk equals 0 percent (closed) and 150 percent (largest) of the area, respectively.

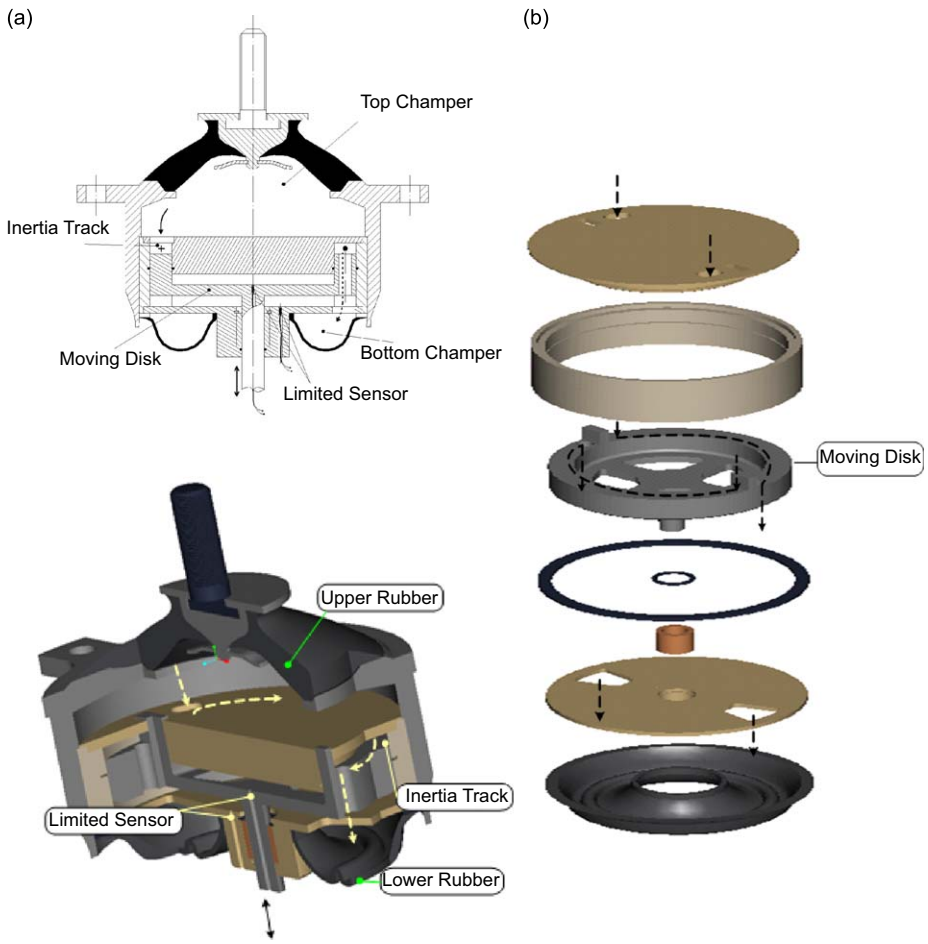

Fig. 1. Hydraulic mount with the variable inertia track: (a) cross section of a hydraulic mount and (b) assembly components.

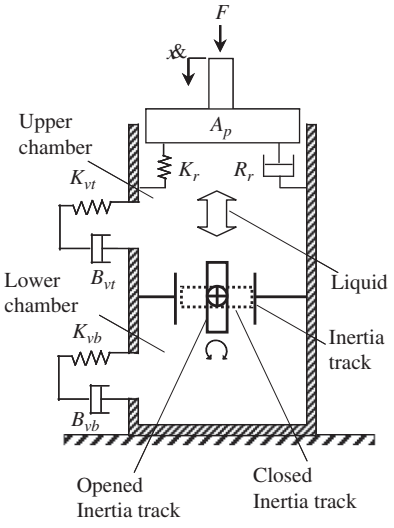

Fig. 2. Mechanical model of the hydraulic mount with the controllable inertia track.

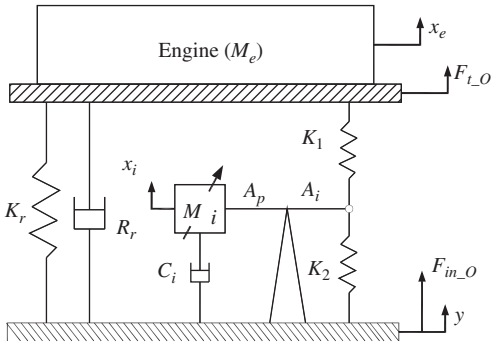

Fig. 3. Mechanical model of the mount (opened inertia track model).

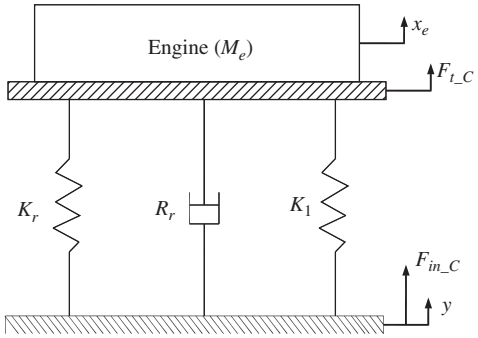

Fig. 4. Mechanical model of the mount (closed inertia track model).

The value 100 percent of the area is the original value which is obtained from the area of the optimal passive hydraulic mount.

A mathematical model of the hydraulic mount is considered in Fig. 2. This hydraulic and mechanical model could then be transferred to a mechanical mode shown in Fig. 3. When the area of the inertia track is closed, the fluid does not flow into the inertia track. Therefore, the model of the mount was changed from the model in Fig. 3 to that in Fig. 4. Here, the volumetric damping of the chambers is neglected by an assumption as B_{vt}=0 and B_{vb}=0.

The motion equations for the opened and closed inertia track models from Figs. 3 and 4 were derived by Newton's law as follows:

$$\begin{bmatrix} M_e & 0 \\ 0 & M_i \end{bmatrix} \begin{Bmatrix} \ddot{x}_e \\ \ddot{x}_i \end{Bmatrix} + \begin{bmatrix} R_r & 0 \\ 0 & C_i \end{bmatrix} \begin{Bmatrix} \dot{x}_e \\ \dot{x}_i \end{Bmatrix} + \begin{bmatrix} (K_r + K_1) & -K_1 \dfrac{A_i}{A_p} \\ -K_1 \dfrac{A_i}{A_p} & (K_1 + K_2)\left(\dfrac{A_i}{A_p}\right)^2 \end{bmatrix} \begin{Bmatrix} x_e \\ x_i \end{Bmatrix}$$
$$= \begin{Bmatrix} 0 \\ M_i \end{Bmatrix} \ddot{y} + \begin{Bmatrix} R_r \\ C_i \end{Bmatrix} \dot{y} + \begin{Bmatrix} K_r + K_1\left(1 - \dfrac{A_i}{A_p}\right) \\ K_2\left(\dfrac{A_i}{A_p}\right)^2 - K_1 \dfrac{A_i}{A_p}\left(1 - \dfrac{A_i}{A_p}\right) \end{Bmatrix} y \tag{1}$$

$$M_e \ddot{x}_e + R_r \dot{x}_e + (K_r + K_1) x_e = R_r \dot{y} + (K_r + K_1) y \tag{2}$$

By using the Laplace transform with zero initial conditions, Eqs. (1) and (2) were calculated as

$$\begin{bmatrix} M_e s^2 + R_r s + (K_r + K_1) & -K_1 \dfrac{A_i}{A_p} \\ -K_1 \dfrac{A_i}{A_p} & M_i s^2 + C_i s + (K_1 + K_2)\left(\dfrac{A_i}{A_p}\right)^2 \end{bmatrix} \begin{Bmatrix} X_e \\ X_i \end{Bmatrix} = \begin{Bmatrix} 0 \\ 0 \end{Bmatrix} \tag{3}$$

$$M_e s^2 + R_r s + (K_r + K_1) = 0 \tag{4}$$

where s is the Laplace operator.

The transmitted forces, F_t for the opened and closed inertia track models based on Figs. 3 and 4 were combined with Eqs. (3) and (4) so as to be obtained

$$F_{t\_O} = (K_r + K_1 + R_r s)X_e - K_1 \frac{A_i}{A_p} X_i \tag{5}$$

$$F_{t\_C} = (K_r + K_1 + R_r s)X_e \tag{6}$$

where

$$X_i = K_1 \left(\frac{A_i}{A_p}\right) \frac{X_e}{M_i s^2 + C_i s + (K_1 + K_2)(A_i/A_p)^2}$$

From Eqs. (5) and (6), the dynamic stiffness, K_t^* for the opened and closed inertia track models was obtained as follows:

$$K^*_{t\_O} = K_{t\_O} + jK'_{t\_O} = \frac{F_{t\_O}}{X_e} = (K_r + K_1 + R_r s) - \frac{\{K_1(A_i/A_p)\}^2}{M_i s^2 + C_i s + (K_1 + K_2)(A_i/A_p)^2} \tag{7}$$

$$K^*_{t\_C} = K_{t\_C} + jK'_{t\_C} = \frac{F_{t\_C}}{X_e} = K_r + K_1 + R_r s \tag{8}$$

The real part, K', of the dynamic stiffness K^*, which represents the stiffness property of the mount, and the imaginary part, K'', which indicates its damping property, were obtained from Eqs. (7) and (8):

$$K'_O = K_r + K_1 - \frac{K_1^2 E(A_i/A_p)^2}{D^2 + (C_i\omega)^2} \tag{9}$$

$$K''_O = R_r\omega + \frac{C_i K_1^2 \omega (A_i/A_p)^2}{D^2 + (C_i\omega)^2} \tag{10}$$

$$K'_C = K_r + K_1 \tag{11}$$

$$K''_C = R_r\omega \tag{12}$$

where $D = (K_1 + K_2)(A_i/A_p)^2 - M_i\omega^2$.

The transmissibility, T_F, for unbalanced vibrations of the engine and the relative transmissibility, T_{RD}, were be obtained from the dynamic stiffness, the real and the imaginary parts of the dynamic stiffness as the following section.

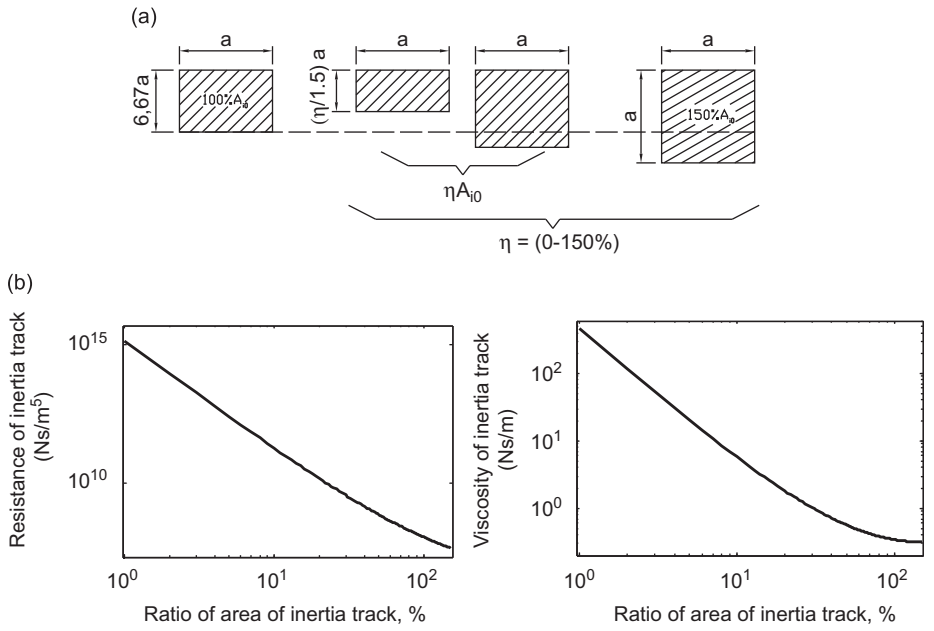

Fig. 5. Area effect of the inertia track: (a) cross-section and variation range of inertia track area; (b) resistance versus the variation of area and (c) viscous damping coefficient versus the variation of area.

3. Dynamic response of the proposed hydraulic mount

3.1. Performance of the inertia track under the area variation

The inertia track of the engine mount is a tube with a specific cross-sectional area and length. Since the amount of fluid mass inside this tube depends upon its cross-sectional area and length, the inertia can be passively varied. As the mount is excited, the fluid will go from the upper chamber to the bottom chamber through the tube and vice versa. Hence, the tube is considered as a fluid resistance which is against the amount of fluid with pumping forces performed by the vibration at the top of the rubber element. In other words, the mass of the fluid in the channel is large enough that infinite force is necessary for its acceleration.

$$T_{RD} = \frac{X_e - Y}{Y} = \left|\frac{-Ms^2}{Ms^2 + K^*}\right| = \frac{M\omega^2}{\sqrt{(K' - M\omega^2)^2 + K''^2}} \tag{13}$$

$$T_F = \frac{X_e}{Y} = \left|\frac{K_O}{Ms^2 + K^*}\right| = \sqrt{\frac{(K'^2 + K''^2)}{(K' - M\omega^2)^2 + K''^2}} \tag{14}$$

The fluid flow going through the inertia track is modeled by using an equivalent orifice of linear fluid resistance R_i, and the fluid resistance is described in [13] as shown below.

The fluid flow going through the inertia track is considered as the linear fluid going through an orifice with an equivalent linear fluid resistance R_i. The fluid resistance is described in [13] as shown

$$R_i = \frac{128\mu L_i}{\pi d_h^4} \tag{15}$$

where μ is the viscosity of the fluid, L_i is the effective length of the track, and d_h is the hydraulic diameter of the track. The hydraulic diameter was calculated by $d_h = 4A_i/P$, where A_i and P are the cross-section and the wetted perimeter of inertia track, respectively. The resistance of the fluid in the track, R_i, is very sensitive with the inertia track area by a fourth equivalent power of the hydraulic diameter.

The cross-section of the inertia track is described in Fig. 5(a). When the area is changed, the resistance $R_i(\eta)$ and the viscosity damping coefficient $C_i(\eta)$ are calculated by Eqs. (16) and (17), respectively.

$$R_i(\eta) = \frac{1.132\mu L_i(\eta + 1.5)^4}{\eta^4 A_{i0}^2} \tag{16}$$

$$C_i(\eta) = R_i(\eta)A_i^2 = \frac{1.132\mu L_i(\eta + 1.5)^4}{\eta^2} \tag{17}$$

where A_{i0} is the inertia track area in the optimal passive mount (η=100 percent); η is the ratio of the inertia track area (0–150 percent).

The relation between the resistance and the viscosity of fluid going through the inertia track are shown in Fig. 5(b) and (c), respectively. When the area increases, the resistance and viscous damping decreases and vice versa.

3.2. Dynamic characteristics of the proposed engine mount

The equations in Section 2 were used in the simulation with the mount parameters listed in Table 1. The results obtained by the simulation show frequency responses of the mount changed according to the variation of the inertia track area.

Table 1
Mount parameters used in the numerical simulation.

Parameters	Original value
A_p	$2.5 \times 10^{-3}\,m^2$
A_{i0}	$5.72 \times 10^{-5}\,m^2$
I_i	$3.81 \times 10^{6}\,N\,s^2/m^5$
L_i	$212 \times 10^{-3}\,m$
ρ	$1.028 \times 10^{3}\,kg/m^3$
μ	$3.67 \times 10^{-2}\,N\,s/m^2$
R_{i0}	$1.05 \times 10^{7}\,N\,s/m^5$
C_1=1/K_{vt}	$3.0 \times 10^{-11}\,m^5/N$
C_2=1/K_{vb}	$2.6 \times 10^{-9}\,m^5/N$
K_r	$2.25 \times 10^{5}\,N/m$
R_r	$100\,N\,s/m$
M	$62\,kg$

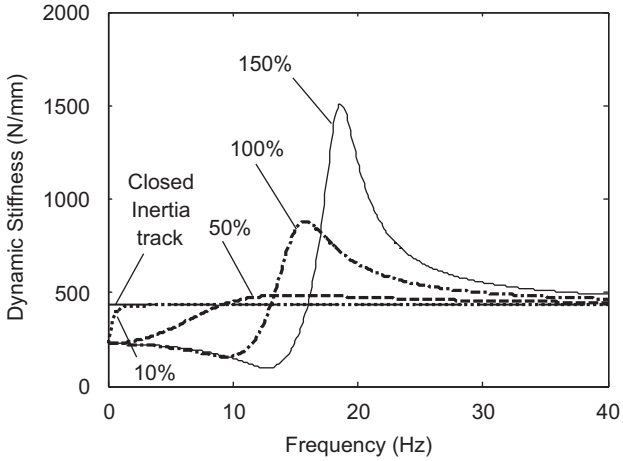

Fig. 6. Dynamic stiffness according to the inertia track area variation.

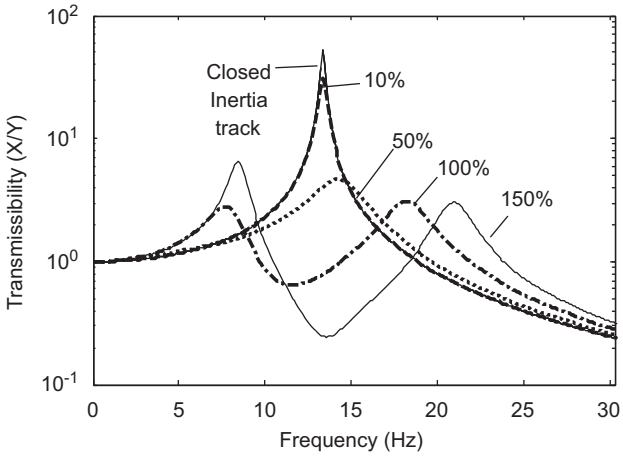

Fig. 7. Transmissibility according to the inertia track area variation.

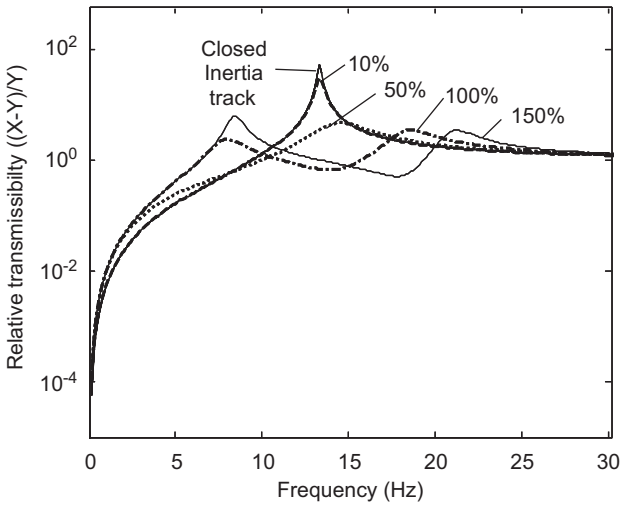

Fig. 8. Relative transmissibility according to the inertia track area variation.

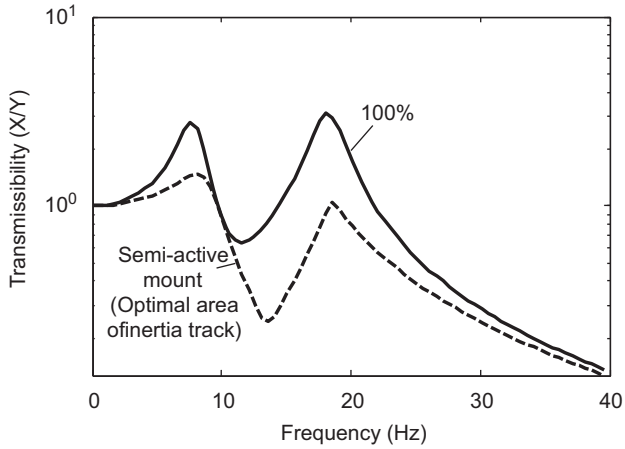

Fig. 9. Transmissibility with the optimal inertia track area.

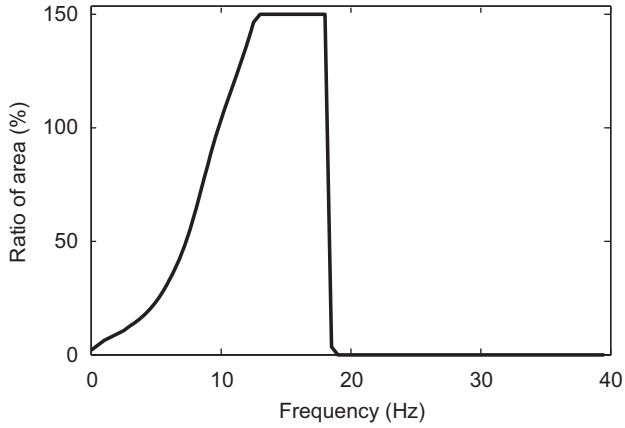

Fig. 10. Optimal area by minimized transmissibility.

Figs. 6, 7 and 8 show the dynamic stiffness, transmissibility and relative transmissibility of the hydraulic mount, respectively. In these figures, the ratio value of the inertia track area is 100 percent which indicates the original area of the optimal passive hydraulic mount.

With an increment of the area, the notch and resonant frequency caused by the fluid flow will increase as shown in Fig. 6. On the contrary, the resonant peak decreases when the area is closed; and when it is almost closed, the resonant frequency is one. As seen in Figs. 7 and 8, two resonant frequencies will appear and change according to the area variation. In this case, the amplitude of the first resonant peak increases while the amplitude of the second resonant peak decreases for an increment of the area.

The optimal area was found by varying the area according to the frequency. In Fig. 9, the transmissibility is greatly reduced, and the optimal area, to minimize the transmissibility, found by considering it change from 0 to 150 percent, is pointed out in Fig. 10.

4. Optimal parameter control algorithm

Many researches based on the reduction of the dynamics stiffness for reducing the transmitted force, while the displacement is not considered. Besides, it is known that the transmissibility expressions for both the force and motion excitations are identical. It would be employed to protect the supporting structure under the force excitation are the same as those were used to protect the dynamic system from the motion excitation. Therefore, the transmissibility minimization is considered for the optimal parameters. In practical, the engine vibration is caused by many disturbance forces as the rotation of unbalance mass, moving of piston, combustion engine, etc. Hence, the effects of a multi-range of excitation force

act to the engine mount will be mentioned. There are two main parameters for describing the signal in the frequency domains that can show the effects on the system. One is the frequency's position, which indicates mainly the frequency band where the signal's energy is located. The other is the frequency's magnitude. In Fig. 10, the transmissibility optimization of a single main frequency domain was depicted but it was not completely with multi-frequencies of the excitation signal which have the similar magnitudes acting on the mount at the same time. Hence, the optimized areas by considering the whole frequencies have to count. Based on the above judgments, an optimal algorithm is suggested to control the inertia track area in order to minimize the summation of the effective transmissibility. The effective transmissibility is a function which includes the main frequencies and their magnitudes.

4.1. Controller

The analysis of the engine vibration by using the fast Fourier transform (FFT) to identify the input signals for the controller includes the frequency position and magnitude. We have a set (B_i,f_i), i=1,2,…,n, where B_i is the magnitude, f_i is the frequency at the ith index. Because, the magnitudes are defined as B_1, B_2,…,B_n and $B_1 \geq B_2 \geq \ldots \geq B_n$, a normalization for the magnitudes $B_{1i}=B_i/B_1$, we have $B_{11}=1$ and $B_{1j} \leq 1$ (j=2…n). From the Eqs. (9)–(12) and (14), we define the transmissibility modulus into the real function as shown below

$$T = \frac{\sqrt{E^2F^2 + E^2H^2 + 4EFH^2 + F^2H^2 + H^4}}{F^2H^2} \tag{18}$$

where

$$E = K_r + K_1 + \frac{\left(\frac{M_i\omega^2K_1A_i}{Ap} - \frac{K_1^2A_i^2}{A_p^2}\right)\left(\frac{A_i^2K_1}{A_p^2} + \frac{A_i^2K_2}{A_p^2} - M_i\omega^2\right)}{\left(\frac{A_i^2K_1}{A_p^2} + \frac{A_i^2K_2}{A_p^2} - M_i\omega^2\right)^2 + C_i^2\omega^2}$$

$$F = K_r + K_1 - M\omega^2 + \frac{\left(\frac{M_i\omega^2K_1A_i}{Ap} - \frac{K_1^2A_i^2}{A_p^2}\right)\left(\frac{A_i^2K_1}{A_p^2} + \frac{A_i^2K_2}{A_p^2} - M_i\omega^2\right)}{\left(\frac{A_i^2K_1}{A_p^2} + \frac{A_i^2K_2}{A_p^2} - M_i\omega^2\right)^2 + C_i^2\omega^2}$$

$$H = B_r\omega - \frac{\left(\frac{M_i\omega^2K_1A_i}{Ap} - \frac{K_1^2A_i^2}{A_p^2}\right)C_i\omega}{\left(\frac{A_i^2K_1}{A_p^2} + \frac{A_i^2K_2}{A_p^2} - M_i\omega^2\right)^2 + C_i^2\omega^2}$$

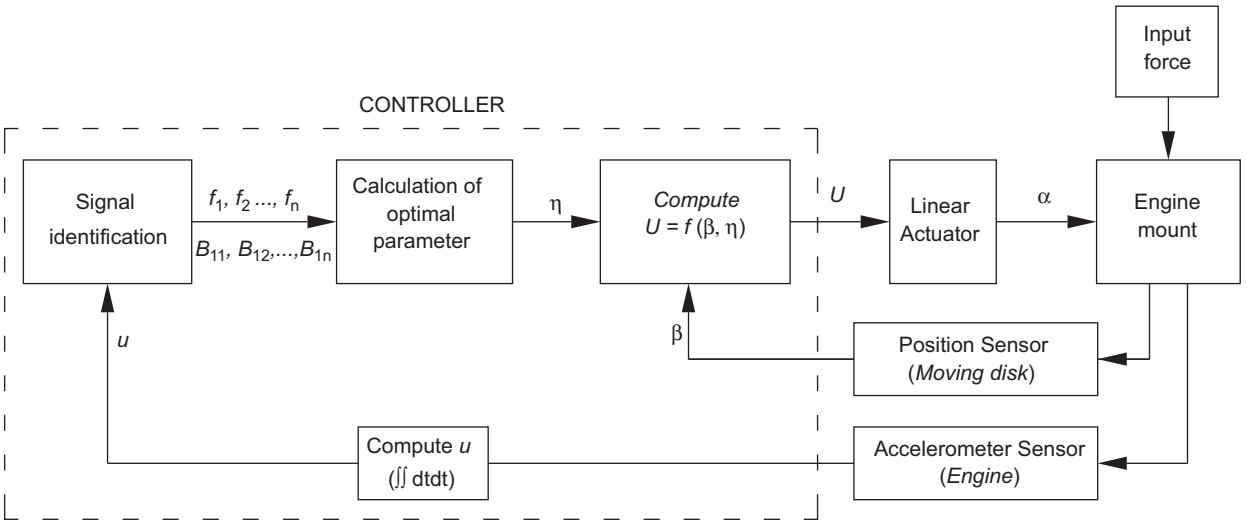

Fig. 11. The control system structure.

By substituting $\omega = 2\pi f$; $A_i = \eta A_{i0}$; $M_i = \rho A_i L_i$ and $C_i = 1.132\mu L_i(\eta + 1.5)^4/\eta^2$ into Eq. (18), a function of the transmissibility, belonging to a frequency and a ratio of area of inertia track, is shown as below

$$T = g(f, \eta) \tag{19}$$

In Eq. (19), the transmissibility $T = g(f, \eta)$ is defined at frequency f and belonged to the ratio of inertia track area η which varies from 0 to 150 percent. The following optimal equation concerning with the effective magnitude is suggested to find out the optimal ratio of the inertia track area η_{OPT}

$$Y(\eta) = \sum_i^n B_{1i} T_i = \sum_i^n B_{1i} g(f_i, \eta) \tag{20}$$

where $g(f_i, \eta)$ is the modulus of the transfer function at frequency f_i related to the ratio of the area of inertia track η, B_{1i} is called as the weighting coefficient by the normalization of magnitude (i=1…n). The effective transmissibility function has the form as $B_{1i}g(f_i, \eta)$. Therefore, the Eq. (20) includes the effect of both the magnitude and the frequency. The optimal area η_{OPT} can be found while $Y(\eta)$ in Eq. (20) is minimal.

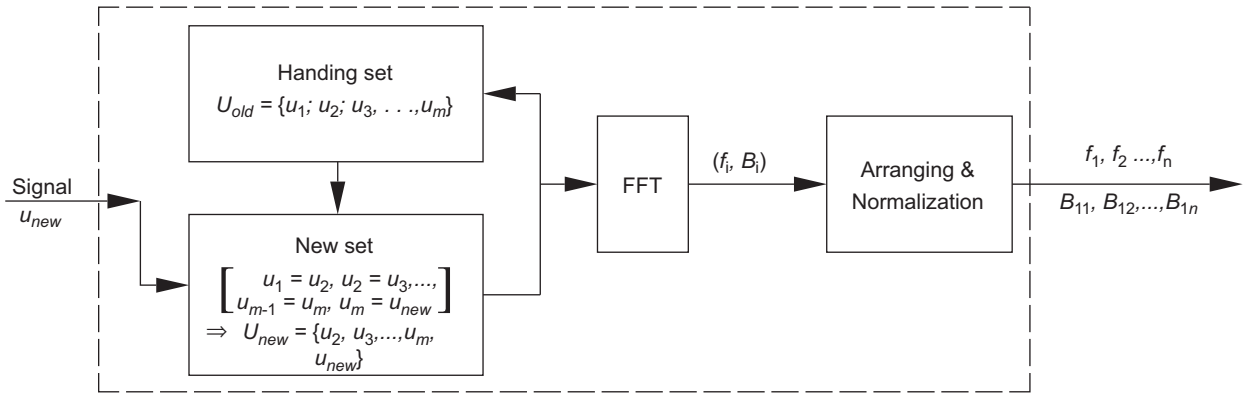

Fig. 12. The structure of the signal identification subsystem.

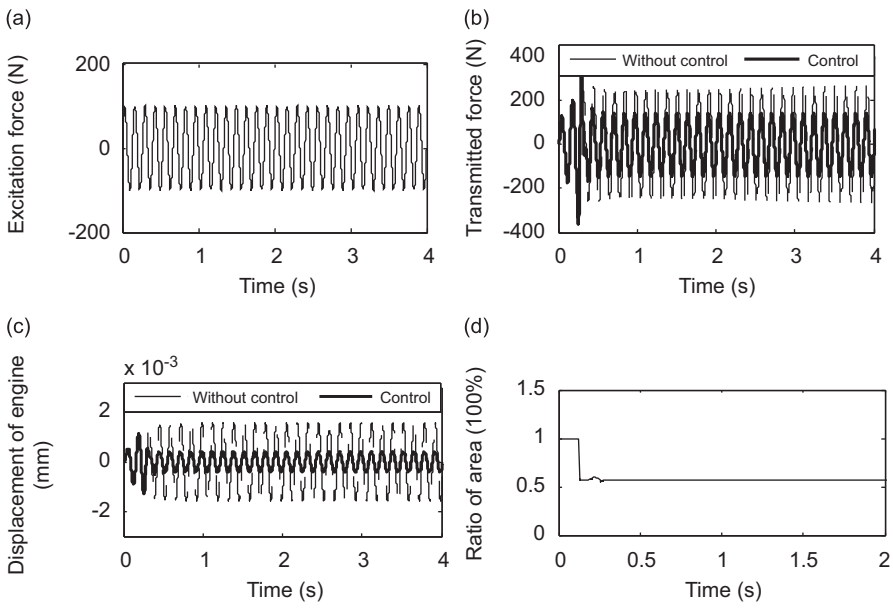

Fig. 13. Control results with respect to a single signal input, at f=7.5 Hz: (a) acting force; (b) transmitted force; (c) displacement of engine and (d) area of inertia track is varied by optimal algorithm.

4.2. Structure of the control system

As shown in Fig. 11, the control system structure consists of three main parts: the identification, the optimal algorithm and the output of control voltage. The identification signal receives the displacement signal of the engine mount and outputs the set of frequencies and weighting coefficients $(B_i f_i)$ i=1,2,…,n, the optimal algorithm finds optimal ratio of area of inertia track η_{OPT} by the minimization Eq. (20). In the simulation, the voltage transmission for the servo motor control is neglected.

The signal identification subsystem shown in Fig. 12 includes three parts: the new handing set, the FFT analyzer and the arranging-normalization part. Because of using the shift index structure of the input signal for the FFT analysis, the output result is updated continuously on route. The shift index structure part is described as a new set. The new set is created by old elements combined with a new element to keep the last and present characteristics of the set. We have U_{new}={u_2, u_3, u_4,…,u_m, u_{new}} and U_{old}={u_1, u_2, u_3,…,u_{m-1}, u_m}, where u_{new} is the new displacement signal of the mount measured by the sensor, U_{new} and U_{old} are defined as the new and old sets with m elements, respectively.

5. Numerical simulation results

As discussed in Section 3.2, the dynamic responses of the mount are shown clearly. By using the optimal area shown in Fig. 10 for a single-signal input, it is possible to find the area for the best vibration isolation response of the mount on the frequency range. On the other hand, it will be not the completive performance for a multi-signal input. In simulation with the parameters given in Table 1, we considered both multi- and single-input signals. By using the optimal Eq. (20) for control, comparisons of the results between the proposed mount and the optimal passive mount were carried out.

5.1. Single-signal of the excitation force

The excitation force which acts on the mount has a sinusoid form, $Fe = 100\sin(2\pi ft)$ (N), where f is frequency of acting force and t is simulation time (t=4 s), is considered. Firstly, at the notch resonance frequency of f=7.5 Hz, the ratio of the optimal area was smaller than 100 percent in this region (Fig. 13). Fig. 13(b) and (c) describe the transmitted force and displacements of the mount, the dotted and continuous lines indicate the optimal passive mount and the proposed mount results, respectively. The input force is shown in Fig. 13(a), and the controlled area is shown in Fig. 13(d). Both of the displacement and the transmitted forces were reduced when the area was adjusted by $\eta_{OPT} \approx 53$ percent. At the beginning, the FFT analyzer was required in order to get enough elements for analysis (256 elements); therefore, we set the area to η=100 percent and then used the optimal algorithm to find the area of inertia track.

Secondly, at a frequency of f=15 Hz, the ratio of the optimal area was larger than 100 percent, η_{OPT}=150 percent, which implies that we would receive the smaller viscosity and the fluid resistance through the inertia track as discussed in Section 3.1. Hence, the displacement restraint was decreased as well as the displacement was increased. With a very small

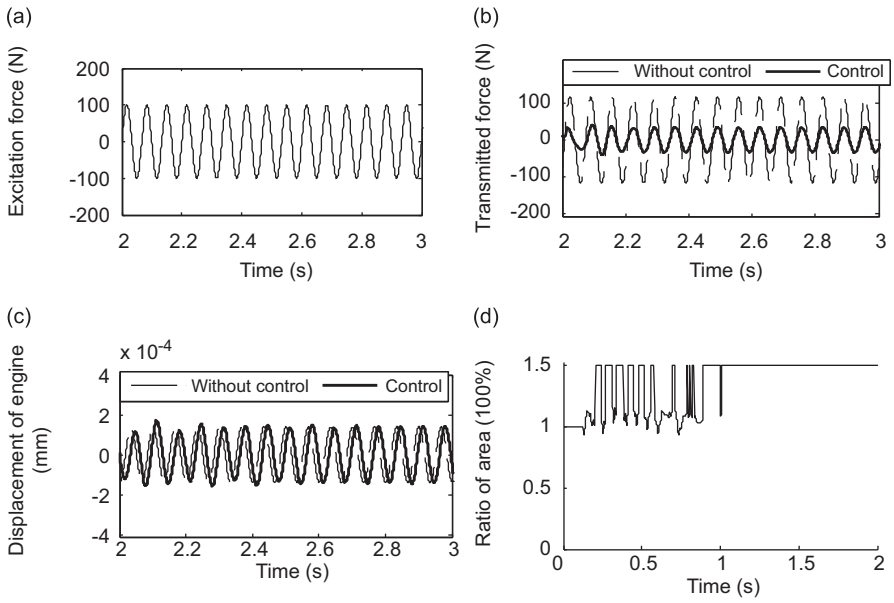

Fig. 14. Control results with respect to a single signal input, at f=15 Hz: (a) acting force; (b) transmitted force; (c) displacement of engine and (d) area of inertia track is varied by optimal algorithm.

increment of the displacement, the transmitted force reduces significantly from 115 to 40 (N), and the results is described in the Fig. 14(b) and (c). Conversely, the displacement did not change, whereas the transmitted force reduced nearly 74 percent, thus clarifying the meaning of the vibration isolation.

By using the single-signal force input, the optimal area was able to be turned to almost the optimal area as shown in Fig. 10. With the single-signal input acting on the mount, we can use the optimal data given in Fig. 10 to control, that means the weighting factors: B_{11}=1 and B_{1j} is very small, $B_{1j} \ll 1$ ($j = 2 \ldots n$). However, in actual, the excitation forces acting on the mount are more complicated by multi-excitation signals with different frequency domains.

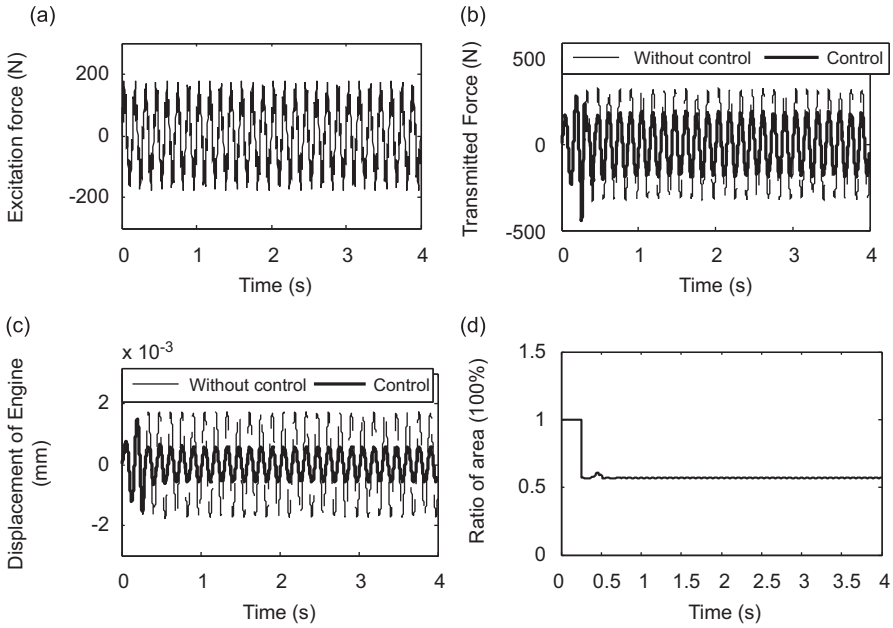

Fig. 15. Control results with respect to a multi-signal input within 0–4 s: (a) acting force; (b) transmitted force; (c) displacement of engine and (d) area of inertia track is varied by optimal algorithm.

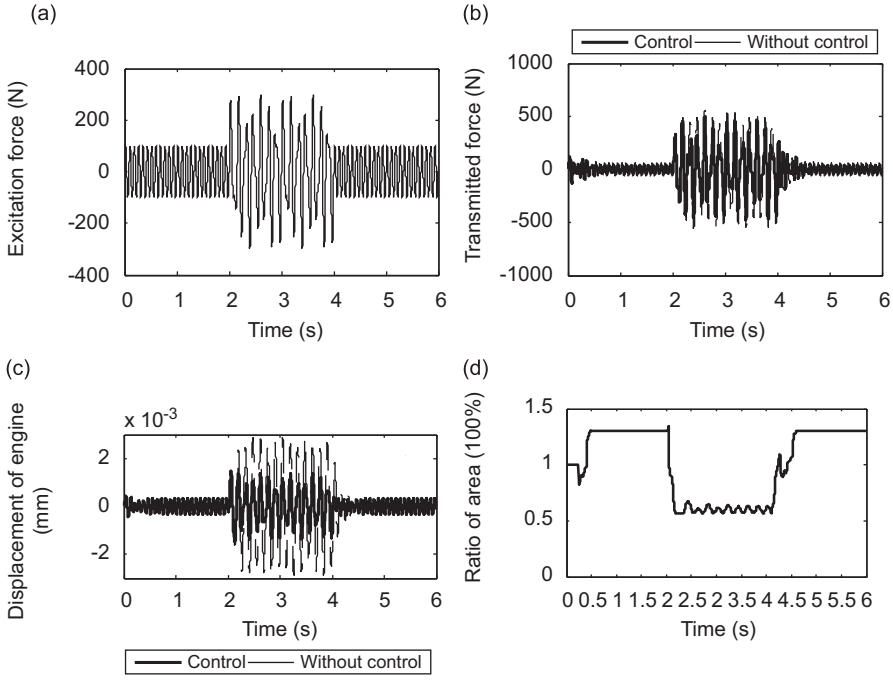

Fig. 16. Control results with respect to the shock force applied form 2 to 4 s: (a) acting force; (b) transmitted force; (c) displacement of engine and (d) area of inertia track is varied by optimal algorithm.

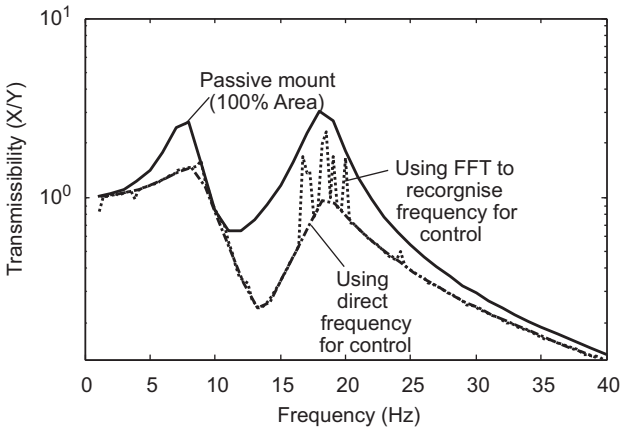

Fig. 17. Transmissibility with respect to the optimal parameter controls.

5.2. Multi-signal of the excitation forces

The engine force is caused by many excitation sources with different frequencies. When analyzing the engine vibration by using FFT, it is possible to find out many different main frequencies which have similar magnitudes. Considering for multi-exciting forces act on the engine in two cases: a stationary signal that is combined by two sinusoidal forms with different amplitudes and frequencies, and a shock vibration with a big amplitude and a low frequency, acting in a short time, that is combined with a stationary sin-wave signal.

Firstly, we assumed that the stationary signal was combined by two sinusoidal acting forces on the mount which had the form $F_e = 130\sin(2\pi 7t) + 50\sin(2\pi 40t)$ (Fig. 15(a)). Fig. 15(b) and (c) show the transmitted force and the engine displacement, respectively. The dotted line denotes the optimal passive system with η=100 percent, while the continuous line denotes the control result with the ratio of optimal area (η_{OPT}) changed by using the optimal algorithm. The optimal area was then turned (Fig. 15(d)).

Secondly, we considered the shock force which has the form as below

$$100\sin(2\pi 12t), 0-2\,\text{s},$$

$$100\sin(2\pi 12t) + 200\sin(2\pi 7t), 2-4\,\text{s},$$

$$100\sin(2\pi 12t), 4-6\,\text{s}.$$

The simulation time was 6 s, the input excitation forces were consisted of a stationary force with the constant frequency applied from 0 to 6 s, and the shock force with the large amplitude and the low frequency was applied from 2 to 4 s. Fig. 16(a) displays the acting force during 6 s. Fig. 16(b) and (c) show the transmitted force and the engine displacement, respectively. The dotted line denotes the optimal passive system, while the continuous line denotes the semi-active control system with η_{OPT} is turned by the optimal algorithm. In Fig. 16(d), the ratio of the optimal area is shown on the control process.

In both the cases, the results show that the transmitted force depicted in Figs. 15(a) and 16(a) and the displacement depicted in Figs. 15(b) and 16(b) are significantly reduced. This proves clearly that the effect of using the semi-active control by the optimal algorithm to turn the area of the inertia track is better than the effect of using the optimal passive system.

5.3. Transmissibility of the mount under control by using the optimal algorithm

As discussion in Section 3.2, the transmissibility described in Fig. 9 with the inertia track area shown in Fig. 10 is the ideal condition for control. Simulation in the steady state with the single signal input, the transmissibility as shown in Fig. 17 in which the dotted lines and the centricity lines are the results with respected to the frequency obtained by the FFT analyzer and the direct frequency, respectively. The controller is very sensitive to the parameter sets which are sent by the FFT analyzer. Therefore, the transmissibility by using the FFT analyzer was a little different with the ideal result where the frequency region is from 16 to 20 Hz. In Fig. 17, it was also found that the optimal transmissibility could be obtained through the method of direct frequency for control.

6. Conclusions

In this paper, a new type of hydraulic engine mount with a controllable area of the inertia track is proposed. The mathematical model of the hydraulic engine mount was derived and utilized during numerical

simulation. The resonant peak, notch and resonant frequencies were changed according to the variation of the inertia track area. By the optimal tuning of inertia track area, the transmissibility of the mount was significantly reduced.

References

[1] G. Kim, R. Singh, A study of passive and adaptive hydraulic engine mount systems with emphasis on non-linear characteristics, *Journal of Sound and Vibration* 179 (3) (1995) 427–453.
[2] P.L. Graf, et al., Modelling and implementation of semi-active hydraulic engine mount, *ASME* 110 (4) (1996) 422–429.
[3] Y. Yu, N.G. Naganathan, R.V. Dukkipati, A literature review of automobile engine mounting systems, *Mechanism and Machine Theory* 36 (2001) 123–142.
[4] G. Kim, et al., Nonlinear analysis of automobile hydraulic engine mount, *ASME* 115 (1993) 482–487.
[5] S. Kazuuo, et al., Optimum design method for hydraulic engine mount, SAE #911055, 1991.
[6] J.E. Colgate, C.-T. Chang, Y.-C. Chiou, W.K. Liu, L.M. Keer, Modelling of a hydraulic engine mount focusing on response to sinusoidal and composite excitations, *Journal of Sound and Vibration* 184 (3) (1995) 503–528.
[7] W.C. Flower, Understanding hydraulic mount for improving vehicle noise, vibration and ride qualities, SAE #88073, 1998.
[8] A.J. Hillis, A.J.L. Harrision, D.P. Stoten, A comparison of two adaptive algorithms for the control of active engine mount, *Journal of Sound and Vibration* 286 (1–2) (2005) 37–54.
[9] T. Shibayama, et al., Active engine mount for a large amplitude of idling vibration, SAE #951298, 1995.
[10] N. Vahdati, M. Ahmadian, Single pumper semi-active fluid mount, ASME & IMECE, 2003.
[11] R. Shoureshi, P.L. Graf, T.L. Houston, Adaptive engine mount, SAE #860549, 1986.
[12] M.S. Foumani, A. Khajepour, M. Durali, A new high-performance adaptive engine mount, *Journal of Vibration and Control* 10 (1) (2004) 39–54.
[13] R. Singh, Dynamic design of automotive systems: engine mount and structure joins, *Sadhana* 25 (113) (2000) 319–330.
[14] G.N. Jazar, M.F. Golnaraghi, Engine mounts for automotive applications: a survey, *The Shock and Vibration Digest* 34 (5) (2002) 363–379.
[15] Y.K. Ahn, B.-S. Yang, M. Ahmadian, S. Morishita, A small-sized variable-damping mount using magnetorheological fluid, *Journal of Intelligent Material Systems and Structures* 16 (2) (2005) 127–133.
[16] Z. Guo, et al., *Robust Identification and Control Design for Engine Mount*, IEEE, London, 1997.